$PbTiO_3$ Nanoparticles Embedded in a Liquid Crystalline Elastomer Matrix: Structural and Ordering Properties

Valentina Domenici,*,†,‡ Blaž Zupančič,‡ Valentin V. Laguta,§,∥ Anatolii G. Belous,⊥ Oleg I. V'yunov,⊥ Maja Remškar,‡ and Boštjan Zalar‡

Dipartimento di Chimica e Chimica Industriale, Università di Pisa, via Risorgimento 35, 56126 Pisa, Italy, Department of Solid State Physics, Jožef Stefan Institute, Jamova 39, 1000 Ljubljana, Slovenia, Ukrainian Academy of Sciences, Institute of Problems in Material Science, UA-03142 Kiev, Ukraine, Institute of Physics, AS CR, Cukrovarnicka 10, 16253 Prague, Czech Republic, and V. I. Vernadskii Institute of General and Inorganic Chemistry, 32/42 Palladiy Ave, 03680 Kiev, Ukraine

Received: April 10, 2010

Ferroelectric $PbTiO_3$ nanoparticles were synthesized to be used as inorganic components of new composite materials based on a liquid crystalline elastomer (LCE) matrix. The preparation and characterization of the composite materials, with a relatively high concentration of $PbTiO_3$ nanoparticles, in the form of thin films is described. The composite films retain the thermomechanical response typical of standard LCEs and the nanoparticles are distributed in the film in anisotropic structures indicating the presence of a coupling between the LCE ordered matrix and the nanomaterials. The nematoelastic coupling and the supercritical nature of the paranematic−nematic transition of the LSCE-based composites was verified also in the presence of ferroelectric nanoparticles.

1. Introduction

Liquid crystalline elastomers (LCEs) belong to the subclass of smart materials called shape memory materials, which typically have the ability to "memorize" the macroscopic shape[1,2] under specific conditions. Several types of shape memory polymeric[3] materials exist based on biopolymers,[4] composites,[5] hydrogels,[6] and liquid crystalline elastomers.[7] Inserting individual nanoparticles in a liquid crystalline elastomeric environment is expected to give to the new composite materials novel properties, like for example the ability to modify the shape by external electric and magnetic fields. There are several examples in the literature[8−13] in which the combination between nanoparticles, such as silica-based or carbon nanomaterials, and nonmesogenic polymeric matrices gives rise to an enhancement of the elastic and mechanical properties of the polymer by itself.[11,12] In recent years, the field of nanostructured composite materials has been developing in a very fast and intense way.[14−18] On the contrary, very little is known about composites made of liquid crystalline polymers and nanoparticles[19,20] and, in particular, about liquid crystal elastomers and ferroelectric/dielectric nanoparticles. Several improvements have been made in preparing LCE composites by using nanotubes,[21] such as carbon nanotubes.[22,23] Different methods have been explored in order to obtain composite films with special electrical properties without losing the peculiar mechanical response of LCEs, but none of them revealed to be successful.[24,25] Conductive composite systems have been recently created by reprocessing standard liquid single crystal elastomer (LSCE) films with carbon nanoparticles through a gel-swelling technique.[26,27] These new materials, consisting of a conductive layer over the surface of the LSCE films, showed interesting properties, such as the piezoresistivity.[28,29] On the other hand, the interest in new functionalized LSCE systems, for instance by introducing azodyes to have photo- and optomechanical effects,[30,31] is rapidly increasing due to the possibility to alter the physical dimensions of the LSCE films (Scheme 1) by a controlled change of the order parameter of the networked mesogen, which is a very promising property for applications as artificial muscles, micropumps, microvalves, and so on.[32,33]

In this work, we have used perovskite-based nanoparticles as ferroelectric inorganic components of the composite materials.[34] Titanates derivatives[11,35] are ceramic systems known for their high piezoelectric activity, ferroelectricity, and dielectric properties.[36−39] In particular, lead-based relaxor ferroelectric ceramics are very attractive materials for actuator applications.[40] The ferroelectricity of lead titanates is the main reason for our interest in this particular material, in addition to our expertise in the field of ceramic relaxors.[41−43] In this paper, the preparation and characterization of polysiloxane-based liquid single crystal elastomers containing highly polarized and electrically active nanoparticles, namely lead titanates ($PbTiO_3$), are reported.[44] In particular, the morphology of both nanoparticles and composite films was investigated by means of Field Emission Scanning Electron Microscopy (FE-SEM). The thermal and thermomechanical responses of the composite films were studied by Differential Scanning Calorimetry (DSC) and thermomechanic measurements, while the ordering properties and thermodynamic nature of the paranematic−nematic transition were detected by Deuterium Nuclear Magnetic Resonance (^{2}H NMR) of a deuterium-enriched LSCE composite film.

2. Experimental Section

2.1. Synthesis of Nanoparticles. Synthesis of $PbTiO_3$ nanopowder was performed by the method of sequential precipitation

* To whom correspondence should be addressed. Fax: 0039-0502219260. Phone: 0039-0502219215. E-mail: valentin@dcci.unipi.it.
† Università di Pisa.
‡ Jožef Stefan Institute.
§ Ukrainian Academy of Sciences, Institute of Problems in Material Science.
∥ Institute of Physics.
⊥ V. I. Vernadskii Institute of General and Inorganic Chemistry.

10.1021/jp103224s
Published on Web 05/27/2010

SCHEME 1: Sketch of the Main Components of the LSCE-Based Composite Films and the Direction of the Local Nematic Director n

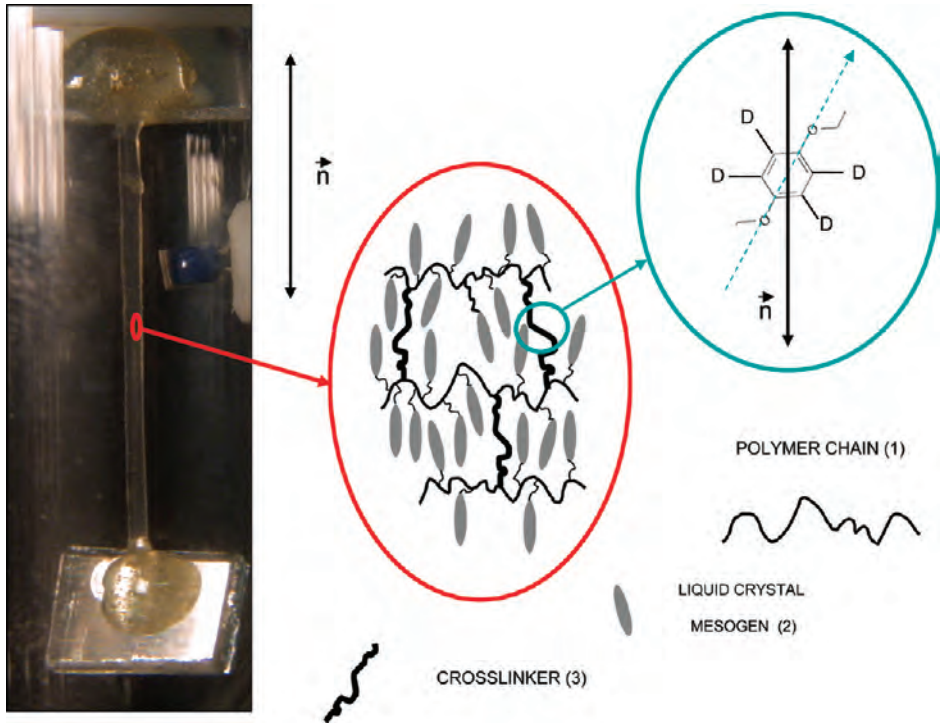

in a 0.1 M water solution of $TiCl_4$ and $Pb(NO_3)_2$. Precipitants were NH_4OH and $(NH_4)_2CO_3$. At the first stage, a certain amount of $TiCl_4$ solution was pumped into a reactor with a constant mass flow. A solution with a pH of 3.9 was stabilized by ammonia. After precipitation of $TiCl_4$, pH in the reactor was increased to 8.5 by adding $(NH_4)_2CO_3$. The precipitate was then intensely mixed for 30 min in the reactor and subsequently for another 30 min in a water bath at 353 K. The $PbTiO_3$ precipitate was dried at 323 K and calcinated for 2 h at different temperatures, from 473 to 1223 K. The composition and morphology properties of the nanopowder were characterized by means of X-ray and FE-SEM techniques, as reported in section 3.

2.2. Preparation of Composite Elastomers. A homogeneous dispersion of $PbTiO_3$ nanoparticles, synthesized as described in section 2.1, in toluene was prepared by mechanical mixing. Different concentrations of nanoparticles were used, ranging from 1% to 5% in weight. A 1 mL sample of such dispersion was added to 1 mL of prepolymerization toluene solution, whose components, reported in Figure 1, are the following: the polymeric chain (**1**) hydroxymethyl-polysiloxane (1 mmol), the mesogen (**2**) 4-methoxyphenyl 4-(but-3-en-1-yloxy)benzoate (0.85 mmol), and the cross-linker (**3**) 1,4-bis(undec-10-en-1-yloxy)benzene (0.075 mmol). Synthesis of components **2** and **3** was performed as described in refs 45−47. The chemical structure and purity of these compounds was checked by means of ^1H and ^{13}C NMR in solution. A commercial platinum catalyst (COD from Wacker Chemie) was added to the final mixture. To produce monodomain LSCE films, we used the well-known two-step cross-linking technique, pioneered by Kupfer and Finkelmann.[45] The prepared mixture was indeed inserted in a circular reactor inside a modified centrifuge. A rate of 4500 rpm and an average temperature of 343 K were set for an hour in order to get a partial cross-linked film-network, still partially wet by the solvent. The second step of the cross-linking reaction consists of slowly removing the solvent under progressive increasing weights at room temperature followed by 3 days of drying at 343 K under constant weight. In this way, we obtained several composite films having similar thickness and shape, with a uniaxial orientation of the local directors, which results in monodomain nano-LSCE stripes. Similar stripes have also been prepared by using a cross-linker (**3**) deuterium-labeled on the phenyl ring as indicated in Figure 1. The purpose was to perform ^2H NMR studies on these composites directly deuterium-enriched in the elastomer matrix. A standard LSCE stripe, without nanoparticles, was also prepared by following exactly the same procedure (without adding the nanoparticle dispersion to the prepolymerization mixture) with the same chemical composition, namely 85% of **2** and 7.5% of **3**. Polydomain samples, obtained without mechanically loading the gel-films during the second cross-linking step, were also prepared. In all cases, the completeness of the cross-linking reaction was checked by means of FTIR spectroscopy, by looking at the disappearance of the typical

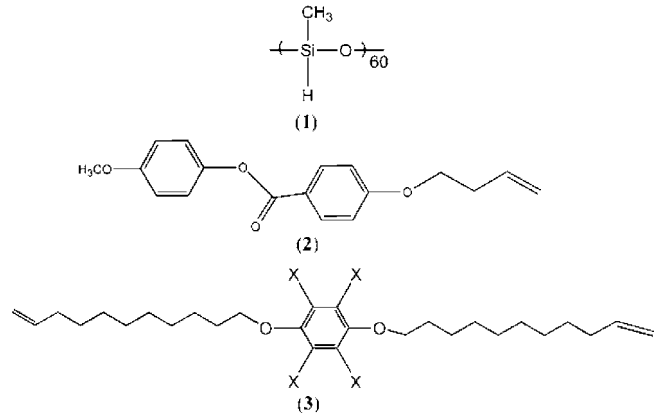

Figure 1. Main components of the LSCE matrix: (**1**) polysiloxane, (**2**) mesogen, (**3**) not labeled cross-linker (X = H) and deuterium labeled cross-linker (X = ^2H).

TABLE 1: Temperatures, *T* (K), Enthalpies, Δ*H* (J/g), and Specific Heat, ΔCp (J/gK), of the Phase Transitions of the Prepared Samples

sample	glass	ΔCp	*T*	nematic	Δ*H*	*T*	paranematic
standard LSCE	√	0.33	269.2	√	2.98	346.8	√
nano-LSCE (1%)	√	0.54	268.1	√	2.02	345.3	√
nano-LSCE (5%)	√	0.45	265.7	√	1.96	344.3	√
nano-LSCE D[a] (5%)	√	0.49	264.1	√	1.86	347.9	√

[a] D is for sample deuterated on the cross-linker (**3**).

Si−H signal ($\tilde{\nu} \approx 2200$ cm^{-1}). All the prepared films were swollen in toluene and dried in the oven at about 320 K. This procedure was repeated several times in order to ensure that no unreacted mesogens or cross-linkers were still present in the network. The absence of unreacted compounds was checked by ^{1}H NMR and FT-IR. The mesophase transition temperatures and enthalpies of the prepared composite films, as determined by DSC, are reported in Table 1.

2.3. Physical and Chemical Characterization. ***2.3.1. Solution NMR Spectroscopy.*** The chemical composition of basic components **2** and **3** needed to prepare both standard LSCE and new composite films was investigated by means of NMR on a Varian VXR 300 spectrometer working at 300 (^{1}H) and 75 MHz (^{13}C) with TMS as internal standard. $CDCl_3$ was used as a solvent.

2.3.2. FT-IR Spectroscopy. Infrared spectra were recorded on a Perkin-Elmer FTIR 1725x spectrometer.

2.3.3. X-ray Diffraction. X-ray Diffraction (XRD) measurements on $PbTiO_3$ nanoparticles were made on a DRON 3 M powder diffractometer (Cu Kα radiation, 40 kV, 18 mA). Structural parameters and phase composition were determined by a Rietveld profile analysis method, by using the Fullprof program[48] and JCPDS Powder Diffraction File data. XRD patterns were run in the angular range $2\theta = 10-100°$ in steps of 0.05°.

2.3.4. Field-Emission Scanning Electron Microscopy. The new materials (both nanoparticles and LSCE composites) have been studied by means of Field-Emission Scanning Electron Microscopy (FE-SEM) with a Supra 35 VP, Carl Zeiss microscope.

2.3.5. Differential Scanning Calorimetry. The mesophase behavior of the new composite materials has been investigated by DSC with a Perkin-Elmer DSC 7 calorimeter. The values of transition temperatures and corresponding enthalpies are given for the second heating and cooling cycle. Each sample was placed into a DSC heating cell at room temperature, cooled to 223 K and after 5 min heated to 415 K, maintained at 415 K for 5 min, cooled to 223 K and after 2 min reheated once again. The heating and cooling rate was 10 deg/min.

2.3.6. ^{2}H NMR Spectroscopy. ^{2}H NMR experiments were carried out on a 9.40 T Varian InfinityPlus400 spectrometer, working at a Larmor frequency of 61.4 MHz for deuterium, with a 90° pulse of 5.9 μs. Temperature was controlled within 0.2°. Thermal equilibration of the sample was 20 min for each temperature. Spectra were recorded as a function of temperature by applying the quadrupolar echo sequence ($90_x-\tau-90_y-\tau-$ACQ) with the EXORCYCLE[49] phase scheme, the delay τ was fixed to 25 μs, and 10 000 scans were acquired for each temperature. A delay between consecutive acquisitions of 200 ms was used.

2.3.7. Thermomechanic Measurements. Thermomechanic measurements have been performed by using a homemade setup, constituted by a temperature-controlled vacuum glass bulb, in which the composite film was hanged, and a camera directly connected with a computer. The variations of the film length were registered as a function of temperature with different heating/cooling rates.

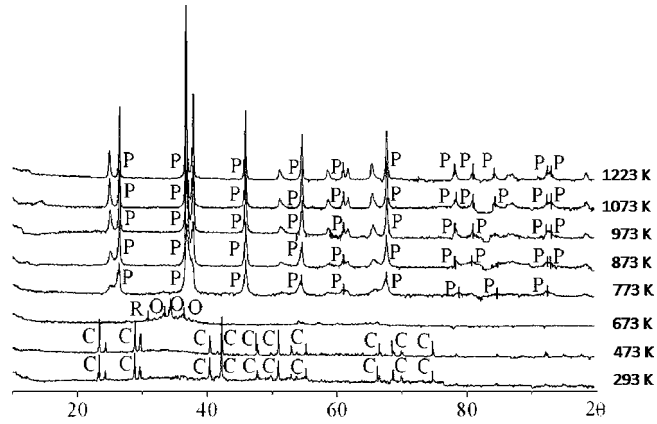

Figure 2. X-ray diffraction patterns of the precipitated $PbTiO_3$ powders calcined for 2 h at different temperatures. C = $PbCO_3$, R = Pb_3O_4, O = Pb_2O_3, P = $PbTiO_3$.

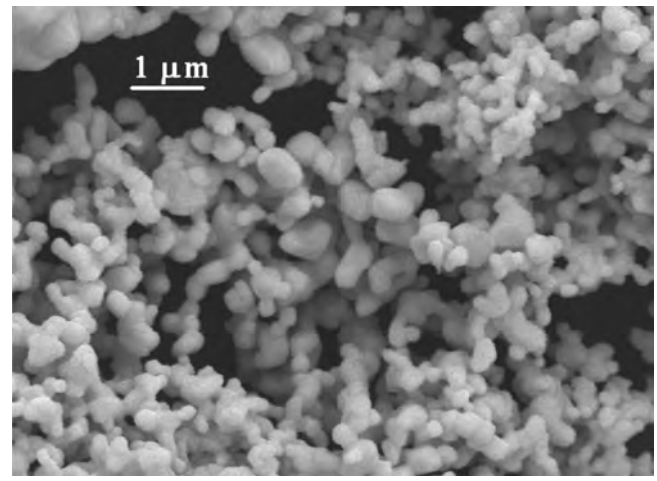

Figure 3. A FE-SEM picture of $PbTiO_3$ quasispherical nanoparticles.

3. Results and Discussions

The $PbTiO_3$ nanoparticles have been synthesized as reported in section 2.1. They were characterized by X-ray Diffraction (XRD) measurements and Figure 2 shows that a pure perovskite phase with tetragonal symmetry appears already at the calcination temperature of 773 K. The size of $PbTiO_3$ nanoparticles (Figure 3) determined by FE-SEM ranges between 800 and 70 nm. Their average shape is slightly elongated and rounded. The nanoparticles are weakly agglomerated in a form of neck-laces.

We have studied the behavior of these nanoparticles diluted in different solvents. In the case of toluene, which is the solvent used for the LSCE preparation, the $PbTiO_3$ nanoparticles start aggregating only after 5−6 h if mechanically mixed for at least 30 min. On the contrary, if ultrasounds are used, the $PbTiO_3$

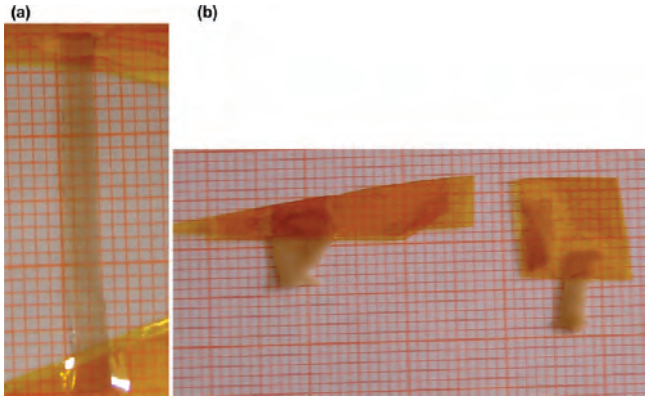

Figure 4. Photographs of (a) a monodomain nano-LSCE stripe containing about 5% of $PbTiO_3$ nanoparticles (nano-LSCE (5%)); (b) two polydomain nano-LSCE stripes containing about 1% of $PbTiO_3$ nanoparticles (nano-LSCE (1%)).

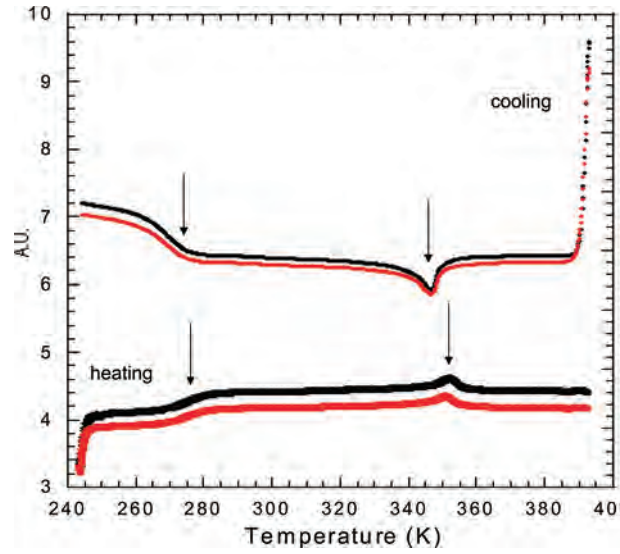

Figure 5. Differential scanning calorimetric curves of the monodomain nano-LSCE (1%) sample under first (black) and second (red) heating and cooling cycles. Black arrows indicate the transition temperatures paranematic−nematic and nematic−glass, as reported in Table 1.

nanoparticles do not agglomerate and form a stable layer at the inner glass surface. For this reason, the preparation of the LSCE composites was performed by mechanically mixing the nanoparticles in the toluene solvent before adding the prepolymerization reactants.

The new LSCE-based composite materials in the form of monodomain films (about 4 cm × 0.4 cm with thickness ∼150−250 μm depending on the samples) were prepared by using different concentrations of $PbTiO_3$. Details of the preparation procedure are reported in section 2.2. Figure 4 shows two photographs of (a) a monodomain stripe of nano-LSCE containing ∼5% in weight of $PbTiO_3$ nanoparticles (nano-LSCE (5%)) and (b) polydomain stripes of nano-LSCE containing ∼1% in weight of $PbTiO_3$ nanoparticles (nano-LSCE (1%)). Both samples are in the nematic phase at room temperature (see Table 1). The color of the stripes is due to the original color of the nanoparticles (yellow ochre). The film displayed in Figure 4a is transparent, thus indicating that the alignment of local nematic directors is homogeneous along the elongation direction: this confirms that the composite film is a monodomain system. On the contrary, polydomain samples (see Figure 4b) are not transparent due to the isotropic distribution of local phase directors, *n*.

The mesophase behavior of the new composite nano-LSCE films was determined by means of DSC. Results are summarized in Table 1. The thermal stability of the prepared composite LSCE films is evidenced by good reproducibility of the DSC curves after first/second heating−cooling cycles (see Figure 5). These results answer important concerns about retaining the thermal properties, in particular the stability of the nematic phase over a wide temperature range and the reproducibility after several heating−cooling cycles. The presence of nanoparticles in different percentages is responsible for a slight shift of the transition temperatures of a few degrees (both paranematic−nematic and nematic−glass phase transition) with respect to the standard LSCE prepared with the same procedure and chemical composition.

The characterization of the distribution of nanoparticles in the nano-LSCE stripes was carried out by means of FE-SEM technique. The presence of single particles indicates that the quasispherical shape of the $PbTiO_3$ nanoparticles enables an easy des-assembly of the observed agglomerates (see Figure 3) by mechanical forces occurring during the film preparation (namely the first step of cross-linking reaction inside the centrifuge). As shown in Figures 6 and 7, the $PbTiO_3$ nanoparticles in the nano-LSCE (with 5% in weight of $PbTiO_3$) films are situated at and near the top-external surface of the film.

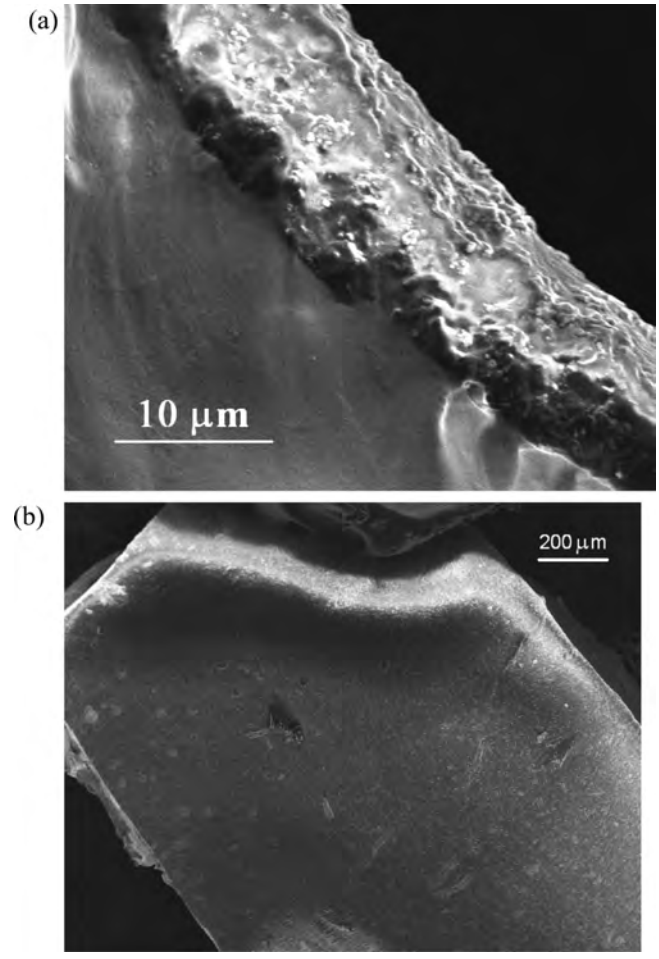

Figure 6. FE-SEM images obtained on a small piece of monodomain nano-LSCE (5%) stripe. The cross-section, or lateral view, of the sample (a) reveals an inhomogeneous distribution of the nanoparticles along the thickness of the stripe, whose total shape is also shown (b).

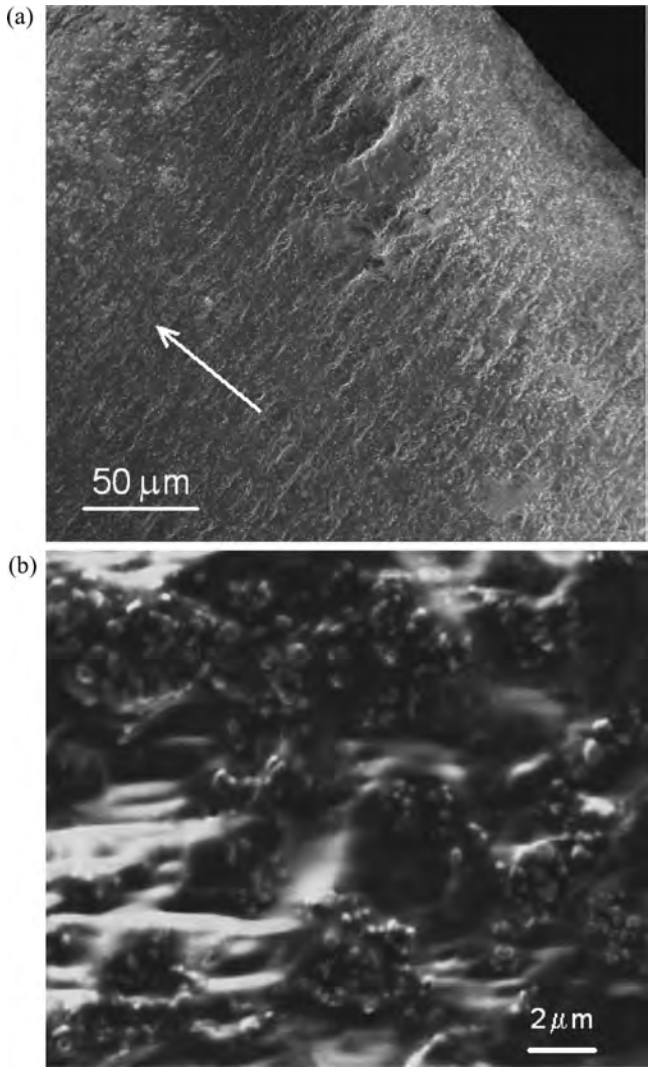

Figure 7. FE-SEM images of the $PbTiO_3$ nanoparticles distributed on the top surface of the nano-LSCE (5%) obtained at different magnifications: (a) 50 and (b) 2 μm. The direction of the nematic director, **n**, is indicated by a white arrow.

The segregation of the nanoparticles near the top surface is caused by the centrifugation process (first step of cross-linking reaction) due to their relatively high molecular weight. The forced sedimentation determines the formation of a thin layer of nanoparticles on the external side of the gel-film, which is then preserved in the next steps of preparation of the final composite films. In Figure 6 it is also possible to see that buckling of the surface and/or nanoparticle penetration causes a modification of the surface layer up to 10 μm in depth. The distribution of $PbTiO_3$ nanoparticles on the top surface shown in Figure 7 is homogeneous and, more significant, there is an evident regular and anisotropic distribution with a particular orientation of nanoparticles with respect to the nematic director, **n**. In fact, FE-SEM microscopy of the top surface of the nano-LSCE (5%) film reveals stripes with des-assembled nanoparticles separated by depleted areas, which might influence the electrothermal response of these new materials. The stripes with a typical period of a few micrometers are perpendicular to the nematic director **n** as reported in Figure 7, where the morphology of the top surface is seen at different magnifications.

The anisotropic distribution of the nanoparticles and their orientation with respect to the nematic director indicates that the particular procedure adopted allows one to obtain a preferred orientation of the nanoparticles due to a coupling between the LSCE orientational order and nanoparticles' orienting properties. In our case, the formation of the network occurs in the presence of nanoparticles which are "free" to move since they are not chemically bonded with any of the polymer units. On the contrary, due to the external mechanical load, which is parallel to the longest dimension of the films (see Figure 4a), the mesogenic units are "forced" to orient along the loading direction. This may lead to preferred distributions of the nanoparticles in terms of free energy of the system.

The transparency of the stripes in the nematic phase indicates the perfect alignment of local domains along the vertical direction. The orientational order of these composite systems was investigated by studying the temperature dependence of the ^{2}H NMR spectra[31,50,51] across the paranematic−nematic phase transition of a monodomain nano-LSCE stripe deuterium labeled directly on the cross-linker (see Figure 1). [So far, ^{2}H quadrupole-perturbed NMR spectroscopy was applied to doped LSCE films with deuterated probes.[50,51]] A selection of spectra is reported in Figure 8. The appearance of the characteristic ^{2}H NMR doublet is observed when gradually cooling the sample from the paranematic phase to the nematic one. As shown in Figure 8 the ^{2}H NMR spectra in the paranematic (far from the transition) and in the nematic phases are well fitted by one and two Lorentzian functions, respectively.

The quadrupolar splitting $\Delta\nu_q$ can be related to the orientational order S of the deuterated moiety according to the following relationship:[52]

$$\Delta\nu_q(T) = \frac{3}{2}q_{aa}\left[S(T)\cdot\left(\cos^2\beta - \frac{1}{2}\sin^2\beta - \frac{\eta}{6}\cos^2\beta + \frac{\eta}{6} + \frac{\eta}{3}\sin^2\beta\right)\right] \quad (1)$$

q_{aa} and η are the quadrupolar coupling constant and asymmetry parameter, respectively. The standard values of $q_{aa} = 185$ kHz and $\eta = 0.04$ have been used in the following analysis.[53] β defines the angle between the CD bond and the para axis of the deuterium labeled phenyl ring, which is fixed to 60° by assuming no distortions from the hexagonal geometry. S is the main orientational order parameter defined with respect to the para axis of the phenyl ring of the cross-linker unit. The biaxiality of the phenyl ring is here neglected. The values of the orientational order parameter S obtained from the analysis of the quadrupolar splittings by using eq 1 are displayed in Figure 9. The trend of S across the paranematic−nematic transition is analogous to those observed for standard LSCE systems[31,50,51] and, in particular, a residual orientational order persists above this transition, as shown in Figure 9. The supercriticality of the paranematic−nematic transition is indeed confirmed also in the presence of nanoparticles on the top surface of the LSCE-based composites. The continuous character of the temperature dependence of S, evidenced by the blue curve in Figure 9, means that the internal mechanical fields, namely the g term in the Landau-de Gennes expression[54] of the free energy density of LSCE systems (see eq 2), is higher than the critical value, g_C.

$$f(T) = f_0 - gS(T) + \tfrac{1}{2}A_0(T - T^*)S^2(T) - \tfrac{1}{3}BS^3(T) + \tfrac{1}{4}CS^4(T) + \ldots \quad (2)$$

Here, the term f_0 is the free energy in the "isotropic" phase ($T\rightarrow\infty$). A_0, B, and C are coefficients related to the symmetry

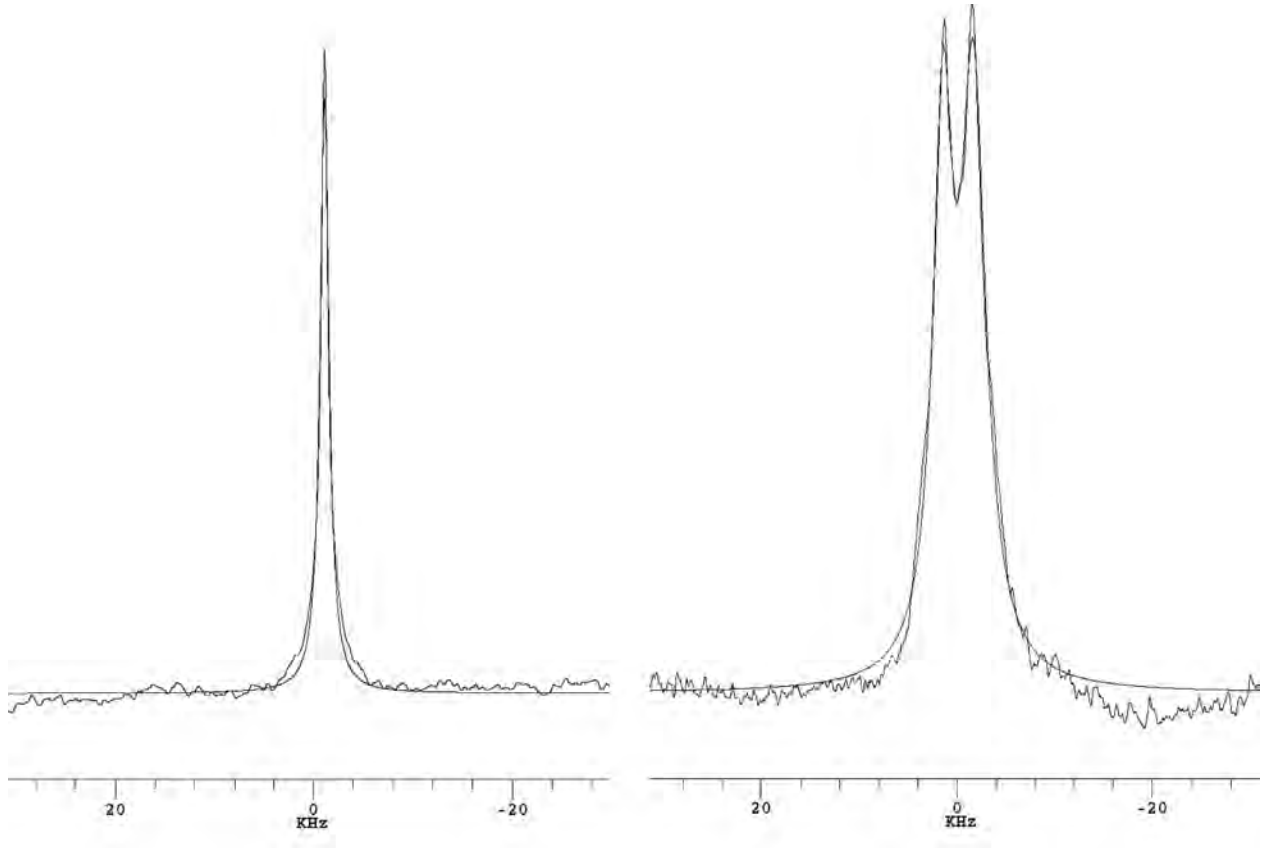

Figure 8. ^{2}H NMR spectra of a monodomain nano-LSCE D (5%) stripe with the nematic director **n** aligned parallel to the magnetic field: (a, left) in the paranematic phase (T = 364 K) and (b, right) in the nematic phase (T = 336 K).

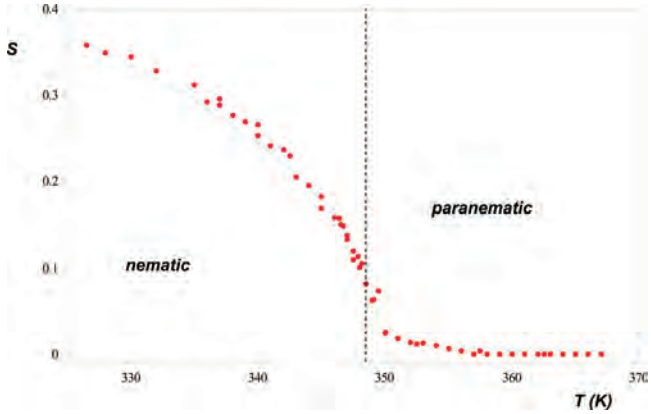

Figure 9. Orientational order parameter S vs temperature T (K) determined by analyzing the ^{2}H NMR quadrupolar splittings as described in the text. The fitting curve obtained according to the Landau-de Gennes theory[54] is in blue. A dashed line is in correspondence with the T* value obtained from the fitting procedure (see eq 2).

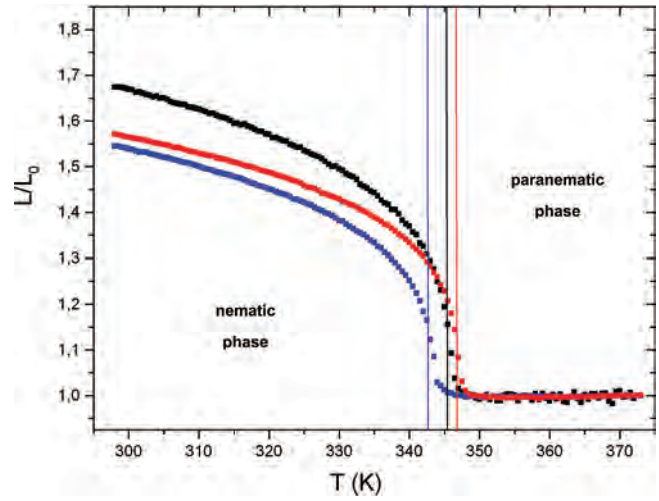

Figure 10. Thermomechanical behavior of the standard monodomain LSCE film (blue symbols), monodomain nano-LSCE (1%) (red symbols), and monodomain nano-LSCE (5%) (black symbols) composite films under the effect of minimal stress (~100 mg). Corresponding colored lines indicate the temperature transition detected by DSC between the paranematic and nematic phases.

of the mesophase and fixed accordingly to thermodynamic quantities (such as the measured latent energy), and T* is the metastable supercooled "isotropic−nematic" temperature transition.[54] In the present case, the fitting of the trend of $S_{zz}(T)$ (Figure 9), according to this theoretical approach,[50,51,54] resulted in a ratio $\boldsymbol{g}/\boldsymbol{g}_C \approx 5$, sensibly higher than in standard LSCEs. The interesting aspect is that the new composite LSCE stripes show a remarkable high orientational order (~0.4 at low temperatures), which is comparable with that measured in standard LSCEs.[50,51] This is also in agreement with the observed high thermomechanical response discussed in the following paragraph.

To prove the preservation of the shape-memory properties in the new composite materials, several thermomechanical measurements under different heating and cooling rates were performed. In Figure 10, the trends of the mechanical elongation ratio ($=L/L_0$) of the nano-LSCE (1%) and nano-LSCE (5%) are compared with that of the standard LSCE prepared with the same procedure and chemical composition. The reproducibility of these trends after several sweeps is

an indication that the addition of nanoparticles does not produce degradation of the films. Moreover, the temperature behavior of the ratio L/L_0 confirms that the nano-LSCE films have a homogeneous orientation of the nematic director. The elongation ($L - L_0$) of the composite film containing the higher concentration of nanoparticles (nano-LSCE (5%)), under minimal stress (~100 mg), is about 55% at room temperature with respect to its length in the paranematic phase (L_0) at $T \rightarrow \infty$. This value is comparable with the elongation of the standard LSCE, which is about 68%, and it proves that the peculiar LSCE shape-memory properties are retained in the nanocomposite films investigated in this work. However, the fact that the elongation of the composite films is less than the standard one induces us to several additional conclusions: (i) The presence on the composite films of a thin layer formed by nanoparticles acts as a reinforcement and partially reduces the ability to extend and therefore the actuation properties of the film. (ii) The composite films prepared in this work show several similarities with the conductive LSCE−nanocarbon systems prepared by Chambers et at.,[26−29] made of a conductive thin layer of carbon nanoparticles on the top surface of a LSCE matrix. However, in our case, the orientation of the nanoparticles on the top surface of the composites indicates the presence of a coupling between the LSCE network and the nanoparticles. (iii) the particular geometry of the composite films and in particular the anisotropic distribution of ferroelectric nanoparticles observed in the present case do not exclude new mechanisms for actuation (i.e., by applying external voltage) by exploiting different geometries (i.e., perpendicular to the thin layer of nanoparticles). This aspect needs further investigation both from the theoretical and experimental point of view, but the results presented here open up new possibilities of application for LSCE-based composites.

4. Conclusions

The preparation and chemical physical characterization of both ferroelectric $PbTiO_3$ nanoparticles and new composite films based on liquid single crystal elastomers (LSCE) and $PbTiO_3$ nanoparticles are reported here. The main conclusions of this work concern the orientational ordering, thermal, and thermomechanical properties of the new composites, as well as the particular distribution of the ferroelectric nanoparticles in the composite films in view of possible technological applications.

Stable LSCE-$PbTiO_3$ nanoparticle composites were prepared by using the well-known two-step "Finkelmann" polymerization technique. DSC curves were recorded to investigate the mesomorphic behavior and confirmed the thermal stability of the new composite systems. ^2H NMR measurements of a composite film deuterium-labeled on the cross-linker showed a rather high degree of orientational order directly related to that of the LSCE matrix thanks to a selective deuteration on the cross-linker units. The thermomechanical measurements performed on several films with different $PbTiO_3$ concentrations indicate that the composite films retain the typical LSCE shape memory property, even though the maximum elongation is slightly less than in standard LSCEs. The concentration profile of the ferroelectric nanoparticles in the elastomeric film is not homogeneous in the volume: their density is higher at the outer surface of the film. The formation of a thin layer rich in $PbTiO_3$ nanoparticles at one side of the films reinforces it and affects the actuation properties of the LSCE composite films evidencing the coupling between ferroelectric nanoparticles and LSCE matrix. This aspect represents a peculiarity of these composite materials in view of actuation mechanisms different from those known for standard LSCE films.

Acknowledgment. V. Domenici and B. Zalar thank the European Commission for the EIF Marie Curie Action project No. 039643 "ELACEM".

References and Notes

(1) Liu, A.; Qin, H.; Mather, P. T. *J. Mater. Chem* **2007**, *17*, 1543.
(2) Chang, L. C.; Read, T. A. *Trans. AIME* **1951**, *191*, 47.
(3) Beloshenko, V. A.; Varyukhin, V. N.; Voznyak, Y. V. *Russ. Chem. Rev.* **2005**, *74*, 265.
(4) Yoshida, M.; Langer, R.; Lendlein, A.; Lahann, J. *Polym. Rev. (Philadelphia)* **2006**, *46*, 347.
(5) Gall, K. D.; Martin, L.; Yiping, L.; Dudley, F.; Mark, L.; Munshi Naseem, A. *Acta Mater.* **2002**, *50*, 5115.
(6) Matsuda, A.; Sato, J.; Yasunaga, H.; Osada, Y. *Macromolecules* **1994**, *27*, 7695.
(7) Warner, M.; Terentjev, E. M. *Liquid Crystal Elastomers*; Oxford University Press: Oxford, UK, 2003.
(8) Lau, K.; Cheng, L.; Su, Z.; Varadan, V. K. *Smart Mater. Struct.* **2009**, *18*, 070201.
(9) El Fray, M.; Boccaccini, A. R. *Mater. Lett.* **2005**, *59*, 2300.
(10) Bandyopadhyaya, R.; Rong, W. Z.; Fredlander, S. K. *Chem. Mater.* **2004**, *16*, 3147.
(11) Dasaroyong, K.; Yeonseok, K.; Kyungwho, C.; Jaime, C.; Choongho, Y. *ACS Nano* **2010**, *4*, 513.
(12) Rossi, G. B.; Beaucage, G.; Dang, T. D.; Vaia, R. A. *Nano Lett.* **2002**, *2*, 319.
(13) (a) Zaborski, M. *Przem. Chem.* **2003**, *82*, 544. (b) Frogley, M. D.; Ravich, D.; Wagner, H. D. *Compos. Sci. Technol.* **2003**, *63*, 1647.
(14) Kasuga, T.; Hiramatsu, M.; Hoson, A.; Sekino, T.; Niihara, K. *Languimir* **1998**, *14*, 3160.
(15) Du, G. H.; Chen, Q.; Che, R. C.; Yuan, Z. Y.; Peng, L. M. *Appl. Phys. Lett.* **2001**, *79*, 3702.
(16) Koch, C. C. *Nanostructured materials; processing, properties, and applications*, 2nd ed.; William Andrew Publisher: New York, 2007.
(17) Hamley, I. W. *Andew. Chem., Int. Ed* **2003**, *42*, 1692.
(18) Dai, H.; Wong, E. W.; Lu, Y. Z.; Fan, S.; Lieber, C. M. *Nature* **1995**, *375*, 769.
(19) Barmatov, E. B.; Pebalk, D. A.; Barmatova, M. V. *Languimir* **2004**, *20*, 10868.
(20) Yaroshchuk, O. V.; Dolgov, L. O.; Kiselev, A. D. *Phys. Rev. E* **2005**, *72*, 011701.
(21) Ahir, S. V.; Terentjev, E. M. *Nat. Mater.* **2005**, *4*, 491.
(22) Courty, S.; Mine, J.; Tajbakhsh, A. R.; Terentjev, E. M. *Europhys. Lett.* **2003**, *64*, 654.
(23) Huang, Y. Y.; Ahir, S. V.; Terentjev, E. M. *Phys. Rev. B* **2006**, *73*, 125422.
(24) Shenoy, D. K.; Thomsen, D. L., III; Srinivasan, A.; Keller, P.; Ratna, B. R. *Sensors Actuators, A* **2002**, *96*, 184.
(25) Kim, K. J.; Shahinpoor, M. *Polymer* **2002**, *43*, 797.
(26) Chamber, M.; Zalar, B.; Remškar, M.; Finkelmann, H.; Žumer, S. *Appl. Phys. Lett.* **2006**, *89*, 243116.
(27) Chamber, M.; Zalar, B.; Remškar, M.; KovaČ, J.; Finkelmann, H.; Žumer, S. *Nanotechnology* **2007**, *18*, 415706.
(28) Chamber, M.; Zalar, B.; Remškar, M.; Finkelmann, H.; Žumer, S. *Nanotechnology* **2008**, *19*, 155501.
(29) Chambers, M.; Finkelmann, H.; Remškar, M.; Sánchez-Ferrer, A.; Zalar, B.; Žumer, S. *J. Mater. Chem.* **2009**, *111*, 524.
(30) Camacho-Lopez, M.; Finkelmann, H.; Palffy-Muhoray, P.; Shelley, M. *Nat. Mater.* **2004**, *3*, 307.
(31) Domenici, V.; Zupančič, B.; Lebar, A.; Umek, P.; Zalar, B.; Ambrožič, G.; Žigon, M.; Čopič, M.; Drevenšek-Olenik, I. *Polymer* **2009**, *20*, 4837.
(32) Yu, Y.; Maeda, T.; Mamiya, J.; Ikeda, T. *Angew. Chem., Int. Ed.* **2007**, *46*, 881.
(33) Madden, J. D. W.; Vandesteeg, N. A.; Anquetil, P. A.; Madden, P. G. A.; Takshi, A.; Pytel, R. Z.; Lafontaine, S. R.; Wieringa, P. A.; Hunter, I. W. *IEEE J. Oceanic Eng.* **2004**, *29*, 706.
(34) Belous, A. G.; Yanchevskii, O. Z.; V'Yunov, O. I.; Mazhara, N. V.; Kovalenko, L. L. *Inorg. Mater.* **2008**, *44*, 414.
(35) Kasuga, T.; Hiramatsu, M.; Moson, A.; Sekino, T.; Niihara, K. *Adv. Mater.* **1999**, *11*, 1307.
(36) Kuwata, J.; Uchino, K.; Nomura, S. *Ferroelectrics* **1981**, *37*, 579.
(37) Park, S. E.; Hackenbergen, W. *Curr. Opin. Solid State Mater. Sci.* **2002**, *6*, 11.

(38) Zhang, H.; Banfield, J. F. *J. Phys. Chem. C* **2007**, *111*, 6621.
(39) Li, J.; Khanchaitit, P.; Wang, Q. *Functional Polymer Nanocomposites for Energy Storage and Conversion*; ACS Symposium Series 1034; American Chemical Society: Washington, DC, 2010; Chapter 4, pp 37−52.
(40) Randall, C. A.; Hinton, A. D.; Barber, D. J.; Shrout, T. R. *J. Mater. Res.* **1993**, *8*, 880.
(41) Blinc, R.; Zalar, B.; Laguta, V. V.; Itoh, M. *Phys. Rev. Lett.* **2005**, *94*, 147601.
(42) Zalar, B.; Laguta, V. V.; Blinc, R. *Phys. Rev. Lett.* **2003**, *90*, 037601.
(43) Blinc, R.; Laguta, V. V.; Pirc, R.; Zalar, B. *Solid State Nucl. Magn. Reson.* **2004**, *25*, 185.
(44) Domenici, V.; Župančič, B.; Remškar, M.; Laguta, V. V.; Veracini, C. A.; Zalar, B. *Artificial Muscles Actuators using Electroactive Polymers*; Advances in Science and Technology series, Vol. 61; Trans Tech Publications: Zuerich, Switzerland, 2009; p 34.
(45) Kupfer, J.; Finkelmann, H. *Makromol. Chem. Rapid Commun.* **1991**, *12*, 717.
(46) Sánchez-Ferrer, A. Ph.D. Thesis, Photo-active liquid crystalline elastomers, Facultat de Quimiques, Departament de Quimica Organica, Barcelona, 2006.
(47) Domenici, V. Unpublished results.
(48) http://www.ill.eu/sites/fullprof/.
(49) Luz, Z.; Meiboom, S. *J. Chem. Phys.* **1963**, *39*, 366.
(50) Cordoyiannis, G.; Lebar, A.; Zalar, B.; Žumer, S.; Finkelmann, H.; Kutnjak, Z. *Phys. Rev. Lett.* **2007**, *99*, 197801.
(51) Cordoyiannis, G.; Lebar, A.; Rožič, B.; Zalar, B.; Kutnjak, Z.; Žumer, S.; Brömmel, F.; Krause, S.; Finkelmann, H. *Macromolecules* **2009**, *42*, 2069.
(52) Veracini, C. A. NMR Spectra in Liquid Crystals the Partially Averaged Spin Hamiltonian. In *Nuclear Magnetic Resonance of Liquid Crystals*; Emsley, J. W., Ed.; Reidel: Dordrecht, The Netherlands, 1985; Vol. 141, Chapter 5.
(53) Domenici, V.; Geppi, M.; Veracini, C. A. *Prog. Nucl. Magn. Reson. Spectrosc.* **2007**, *50*, 1.
(54) de Gennes, P. G. *C. R. Acad. Sci.* **1975**, *281*, 101.

JP103224S